Miniature Otto Prism Coupler for Integrated Photonics

Kirill R. Safronov, Vladimir O. Bessonov,* Daniil V. Akhremenkov, Maxim A. Sirotin, Maria N. Romodina, Evgeny V. Lyubin, Irina V. Soboleva, and Andrey A. Fedyanin

One of the main issues in integrated photonics is the coupling of free-space or optical fiber radiation to waveguides on the photonic chip surface. The ideal coupler is miniature, highly efficient, and provides a large number of addressable devices. Here, a new concept of 3D out-of-plane coupler is introduced, which is a microscale prism exploiting frustrated total internal reflection in the Otto configuration to excite surface electromagnetic waves or near-surface waveguide modes. A method for designing the couplers operating at normal incidence is proposed and it is applied to excite Bloch surface waves (BSWs) in 1D photonic crystals. Polymer microprisms are printed using two-photon laser lithography and allow transferring more than 40% of the incident light energy into BSWs. The couplers enable focusing BSWs simultaneously with their excitation. Advanced design prisms can provide nearly 100% efficiency, making the proposed concept an alternative to actual coupling concepts in integrated photonics.

1. Introduction

Integrated photonics is an actively developing field providing robust scalable platforms to implement complex functionalities for lab-on-chip,[1] quantum optics,[2] and even deep learning[3] applications. Miniaturization of optical chips requires subwavelength light confinement using either narrow step-index waveguides[4–6] or surface electromagnetic waves[7–10] (SEWs) allowing reducing the waveguide mode size to tens of nanometers.[11] However, the typical mode-field diameter of light propagating in optical fibers or in free space is much larger than the wavelength of light and hence the size of the waveguide modes propagating in photonic platforms. This mode mismatch presents a great challenge for efficient and compact coupling of light to waveguides on optical chips and imposes the need to develop special devices named optical couplers.

Optical couplers can be in-plane and out-of-plane. Their coupling efficiency is defined as the percentage of light energy transferred to the waveguide mode. In the case of in-plane couplers, light propagates along the chip plane and enters a waveguide through its edge at the chip facet. Effective coupling is achieved by realizing the field distribution at the entrance to the waveguide as close as possible to the lateral field distribution of the waveguide mode, which is usually Gaussian for conventional platforms. Such couplers provide wide spectral bandwidth and high efficiency, which typically exceeds 80% and can reach higher values, as has been shown for surface plasmon–polariton[12] (SPP) and silicon-on-insulator[13–15] (SOI) platforms. However, in-plane couplers require precise alignment[16] and need to be placed close to the chip edge,[17] which reduces the number of addressable waveguides and significantly limits the applicability of in-plane couplers in densely packed photonic chips.

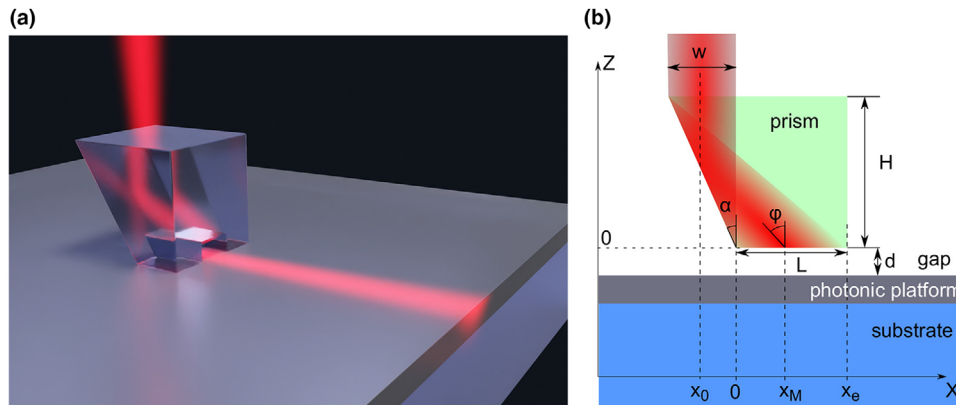Out-of-plane couplers inject incident light into a waveguide by modifying the direction and/or magnitude of the wavevector. Out-of-plane couplers can be implemented in analogy to edge couplers using mode matching, whereby the end of the waveguide is bent and pulled out of the plane of the chip surface.[18–21] More preferred, however, are compact grating couplers that use a phase-matching mechanism to excite waveguide modes with any mode-field profile. Although gratings can be fabricated together with waveguides in a single fabrication procedure, they always direct part of the light into the substrate, exhibiting moderate directionality.[16] Grating coupling efficiency up to 87% can only be obtained using oblique incidence,[22] apodized configuration,[23] backreflecting mirrors,[24] subwavelength structuring,[25,26] and optimization process.[27] As a result, high-performance gratings[28] require time-consuming optimization and complex multi-stage manufacturing with the highest possible precision.

Another type of out-of-plane couplers utilizing a phase-matching mechanism are prism couplers that match the projection of the incident light wavevector with the waveguide mode wavevector. Prisms are often used to excite SEWs whose typical mode-field distribution is significantly different from Gaussian, meaning that they are unlikely to be efficiently excited with in-plane couplers. Prism couplers provide nearly 100% directionality and coupling efficiency in theory and demonstrate in the experiment an efficiency exceeding 90% even for high-index waveguides.[29] Prism couplers can also be successfully applied for SOI waveguides.[30,31] The simple and popular Kretschmann configuration[32] assumes the optical contact of the prism to the platform substrate implying that the materials of the photonic chip must be transparent at the operating wavelength. This

K. R. Safronov, V. O. Bessonov, D. V. Akhremenkov, M. A. Sirotin, M. N. Romodina, E. V. Lyubin, I. V. Soboleva, A. A. Fedyanin
Faculty of Physics
Lomonosov Moscow State University
Moscow 119991, Russian Federation
E-mail: bessonov@nanolab.phys.msu.ru

The ORCID identification number(s) for the author(s) of this article can be found under https://doi.org/10.1002/lpor.202100542

ADVANCED
SCIENCE NEWS
www.advancedsciencenews.com

LASER
& PHOTONICS
REVIEWS

www.lpr-journal.org

Figure 1. Concept of a microprism coupler. a) Schematic of the coupler. A light beam falls on the microprism at normal incidence, reflects off the slanted face, and hits the air gap between the prism base and the waveguide surface of an optical chip. A waveguide mode or surface electromagnetic wave is excited under the prism base due to the phase matching condition through frustrated total internal reflection. At the end of the gap, the waveguide mode under the prism is converted into a waveguide mode that freely propagates along the surface of the platform or in the waveguide on it, thus implementing highly efficient unidirectional coupling. b) Coupling scheme with designations. Main parameters of the prism that should be optimized to obtain maximum coupling efficiency are the gap thickness d, angle of incidence φ, and the position of the beam center x_M.

limitation is circumvented by using the Otto configuration,[33] in which the prism is separated from the waveguide surface by a gap on the order of a wavelength, filled with air or low-index material. This makes the Otto configuration beneficial for practical use, but significantly complicates its implementation because of the need to control precisely the gap thickness. Being almost ideal couplers for SEW platforms, conventional prism couplers are centimeter-sized and require oblique incidence of light, making them incompatible with the concept of integrated photonics.

In this paper, we propose the concept of an integrated microprism coupler that implements the Otto configuration for focused beams incident normal to the optical chip surface. The coupler size is scaled according to the size of the beam and is typically two to three beam diameters. We demonstrate the coupler for the Bloch surface wave (BSW)[8] platform that is all-dielectric counterpart to SPP one, but has the advantages of long propagation length[34] and ultrawide spectral range of operation (from UV[35] to mid-IR[36]), making BSW applicable for integrated photonics,[10,37–39] sensing,[40–42] and other fields.[43–49] Microprism couplers are printed on the surface of a photonic crystal using two-photon laser lithography[50] (TPL) capable of creating efficient in-plane[17] and out-of-plane microcouplers[19–21] operating on the mode-field matching principle. The proposed microprisms use phase-matching mechanism and show the coupling efficiency of 73% in theory and more than 40% in the experiment, which is several times higher than the previous achievement obtained with a grating[51] for the BSW platform.

2. Results and Discussion

2.1. Design Method

We discuss the method of designing microprisms for SEW platforms, but all the considerations below are also suitable for conventional waveguide platforms. The schematic of the coupler is shown in **Figure 1**. The prism is made of a transparent material with a refractive index n_{pr} and has a trapezoidal shape with an air gap region of thickness d between the prism base and the surface

of an integrated photonic platform supporting SEWs or waveguide modes with an evanescent electromagnetic field in air. A light beam with a diameter w falls on the upper face of the prism at the normal incidence, then reflects off the slanted face due to total internal reflection and hits the prism base, where the conventional prism coupling in Otto configuration takes place. The angle of incidence φ on the prism base exceeds the critical angle, leading to phase matching of the incident beam with SEW and, as a result, to the energy transfer through the overlap of the evanescent incoming light and SEW field inside the air gap. Simultaneously with the coupling process, the propagating SEW leaks back into the prism implying that the position x_M of the beam on the prism base should be quite close to the prism edge x_e to terminate the decoupling process and store the energy in SEW. The maximum coupling efficiency is achieved due to the best compromise between the coupling and decoupling processes by proper choosing d, φ, and x_M values for a given beam diameter w and type of photonic platform.

We consider an incident Gaussian beam and a uniform air gap. The theory of prism coupling for this case is detailed by Ulrich in ref. [52] for thin-film waveguides and is applied here for SEWs. The SEW propagation is described by its complex effective refractive index $n_{eff} = Re(n_{eff}) + iIm(n_{eff})$, which depends on the light frequency in accordance with the SEW dispersion law. The real part, $Re(n_{eff}) = k_{SEW}/k_0$, depicts the SEW phase velocity, where k_{SEW} is a SEW propagation constant, k_0 is a wavenumber of the incident radiation in vacuum. The imaginary part $Im(n_{eff})$ reflects SEW losses including absorption and leakage radiation. The SEW excitation is characterized by the resonance in the peak amplitude of the mode field, which has a Lorentzian lineshape[52] and can be written in terms of incidence angles φ for the case of prism coupling

$$\max|E|^2 = \frac{Const}{(n_{pr} \sin \varphi - Re(n_{eff}))^2 + (Im(n_{eff}))^2} \quad (1)$$

The resonance maximum corresponds to the phase-matching condition $n_{pr} \sin \varphi_{ex} = Re(n_{eff})$ fulfilled for an particular inci-

dence angle $\varphi = \varphi_{ex}$, while the resonance's full width at half maximum is $2Im(n_{eff})$. The presence of the prism near the chip surface changes propagation properties of SEW making n_{eff} dependent on the gap thickness. A decrease in the gap thickness leads to an increase in the $Im(n_{eff})$ value, that is, to additional losses due to leakage into the prism, as well as to a shift of the SEW resonance, that is, to a change in the values of $Re(n_{eff})$ and excitation angle φ_{ex}. The condition for achieving peak coupling efficiency determines the gap thickness d and is written in terms of SEW effective refractive index[52,53] (Section S1, Supporting Information)

$$w = \frac{2\cos(\varphi_{ex}(d))}{1.46\,k_0\,Im(n_{eff}(d))} = \frac{\cos\left(\arcsin\left(Re(n_{eff}(d))/n_{pr}\right)\right)}{0.73\,k_0\,Im(n_{eff}(d))} \tag{2}$$

This condition actually means that for optimal coupling, the angular width of the resonance of SEW propagating under the prism should be approximately equal to the divergence of the incident beam. In turn, the SEW angular width increases with a decrease in the gap, making it possible to implement the optimal coupling for almost any beam diameter. When the prism base length $L \gg w$ and Equation (2) is met, the coupling efficiency reaches a maximum value of 80% for a distance between the beam center and the prism edge[52]

$$x_e - x_M \approx 0.37w/\cos(\varphi_{ex}) \tag{3}$$

Equation (3) implies that the beam should be cut off at the right edge of the prism (see Figure 1b) to prevent the transfer of SEW energy back into the prism, which begins to dominate over the coupling process with increasing $x_e - x_M$. For practical applications, the prism base should be as short as possible, provided the beam is not clipped significantly by the left edge of the prism. Thus, it is reasonable to set the base length on the order of the beam diameter on the prism base: $L \approx w/\cos(\varphi_{ex})$. Finally, the prism height $H \geqslant L\cot(\alpha)\cos(2\alpha)$, angle $\alpha = \varphi_{ex}/2$ of slope of the slanted face, and the beam position $x_0 = x_M \tan\alpha/(\tan 2\alpha - \tan\alpha)$ on the prism upper face are found from simple geometric considerations.

We summarize the prism design method that is suitable for both SEW and conventional waveguide platforms as follows.

1. Calculate the dependence of the maximum field on the angle of incidence φ and the thickness d of the gap. Calculations can be done using common computing techniques such as transfer matrix method[54] (TMM) for the 1D case of a multilayer structure containing layers of a photonic platform and two semi-infinite media as a prism and a substrate.
2. Approximate the waveguide mode angular resonance by Equation (1) for each gap and obtain the values of φ_{ex} and $Im(n_{eff})$ depending on the gap thickness d.
3. Solve Equation (2) and find the optimal gap thickness d and excitation angle φ_{ex} for a given diameter w of the beam.
4. Find the optimal position x_M of the beam using Equation (3) and obtain other parameters of the microprism of the desired design using geometric considerations.

The Equations (1)–(3) are valid for both 1D and 2D Gaussian beams.[52] Note that the above theory does not take into account

the mismatch of the waveguide modes propagating under and outside the prism. The field distribution mismatch at the abrupt end of the gap leads to scattering of part of the mode energy and to a decrease in the total coupling efficiency. These additional losses can be determined by any conventional numerical method (FDTD, FEM, etc.). Despite the ability of the method to very quickly determine the optimal parameters of the coupler, there are a number of limitations under which the refinement of the parameters using numerical simulation may be required (Section S2, Supporting Information). Here we apply the design method for the BSW platform. The example of the coupler for SPP platform is described in Section S3, Supporting Information.

2.2. Microprism Design for BSW Platform

We design the microprism coupler for a Gaussian beam with a diameter of $w = 10\,\mu m$ and a wavelength of $\lambda_0 = 780$ nm, which are used in the experiment. As a BSW platform, 1D photonic crystal (PC) is utilized consisting of ten pairs of alternating layers of SiO_2 and Ta_2O_5 sputtered on a glass substrate. PC sustains TE-polarized BSWs for the near-IR wavelength range.

We use TMM in the first optimization step. The scheme of the structure under study is shown in **Figure 2**a. TE-polarized plane wave falls on the structure from the side of the prism that is a semi-infinite layer with a refractive index $n_{pr} = 1.5$ corresponding to the refractive index of the polymer[55] used in the experiment. BSW is detected by a dip in the reflectance spectra (Figure 2b) calculated for the gap thickness $d = 1\,\mu m$. For $\lambda = 780$ nm we found the BSW parameters $Re(n_{eff}) = 1.092$ and $\varphi_{ex} = 46.7°$. These parameters are very close to that of BSW on a bare PC, since the prism has almost no effect on BSW due to the large gap thickness (Section S4, Supporting Information). The BSW field distribution normalized to the incident field is shown in Figure 2a with a red curve, from which the maximum field value $\max|E|^2$ can be obtained. We calculate the field distribution in the structure for the angles of incidence in the vicinity of 46.7° and the gap thicknesses starting from 100 nm. As the result, $\max|E|^2$ as a function of φ and d is obtained in Figure 2c revealing the BSW resonance. The resonance width increases with decreasing gap thickness, indicating an increase in radiation losses due to BSW leakage into the prism. At the same time, the angle φ_{ex} reduces with gap decreasing. For each gap thickness, we approximate the BSW angular resonance by Equation (1) and extract the dependences $Re(n_{eff}(d))$ and $Im(n_{eff}(d))$. Substituting these values in Equation (2) we find its solution in terms of gap thickness and beam width, which is shown in Figure 2d. Dashed lines display the case of the 10 μm beam width corresponding to the gap thickness of 280 nm, at which the maximum coupling efficiency of 80% is theoretically achievable. The inset in Figure 2d depicts the result of BSW resonance approximation by Equation (1) for $d = 280$ nm, giving $\varphi_{ex} = 46.2°$. Next, we determine $x_e - x_M = 5.3\,\mu m$ from Equation (3) and then find the face slope angle $\alpha = 23.1°$, the prism base length $L \geq 14\,\mu m$, and the prism height $H \geq 23\,\mu m$.

We verified the obtained optimal coupling parameters by performing 2D numerical simulation using TMM with plane wave expansion (Experimental Section). This method allows us to properly take into account the effects associated with beam fo-
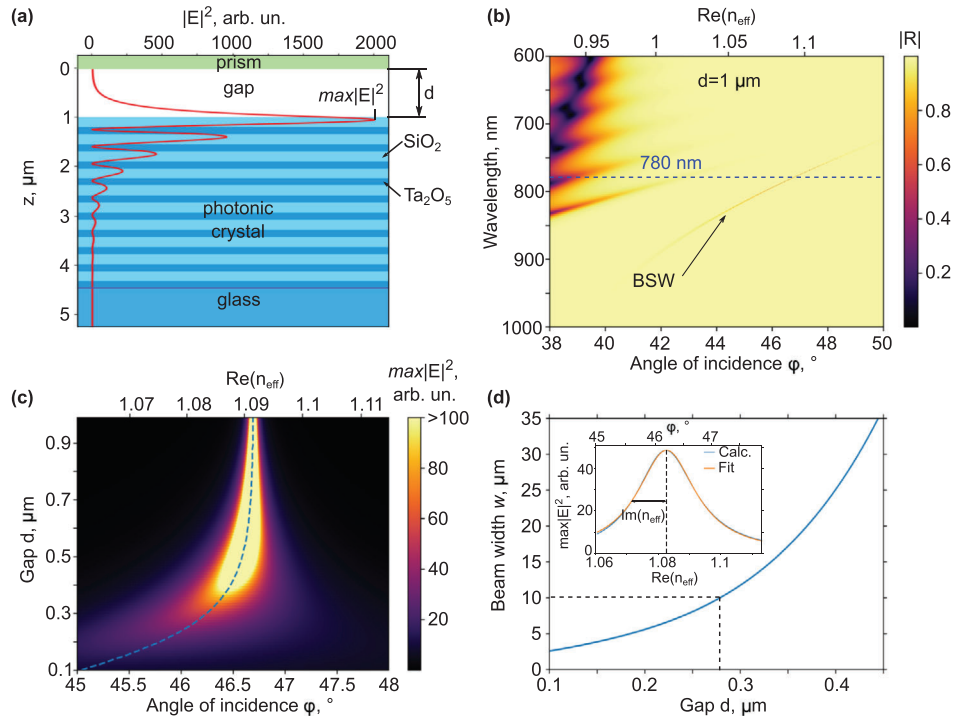
Figure 2. Optimization of coupler parameters. a) Scheme of the 1D multilayer structure corresponding to the system under study. TE-polarized plane wave falls on the system from the side of the prism. BSW field distribution at $\lambda = 780$ nm is shown by a red curve. b) Dependence of the reflection coefficient of the system on the wavelength and angle of incidence, calculated for the air gap $d = 1$ µm. The reflectance dip signifying BSW excitation is marked by an arrow. A blue dashed line indicates excitation radiation wavelength used in the experiment. c) Dependence of maximum $|E|^2$ value on the gap thickness and angle of incidence. Dashed line shows the position of the BSW resonance center. d) Dependence of the beam diameter on the gap thickness for the case of maximum coupling efficiency of about 80%. Black dashed lines indicate the diameter of the Gaussian beam in the experiment and the corresponding optimal gap of 280 nm. Inset shows Lorentzian approximation of $\max|E|^2$ angle dependence for $d = 280$ nm.

cusing and to refine the optimal parameters of the prism, which is especially important for cases of tight focusing, when the analytical theory becomes inaccurate (Section S2, Supporting Information). An example of a 2D electric field distribution $|E(x,z)|^2$ for the case of optimal coupling is shown in **Figure 3**a. The beam is focused on the base of the prism at the point $x_M = 0$. As BSW propagates under the prism, the amplitude of the BSW field first increases to its maximum at the point x_{max} and then decreases due to leakage back into the prism. The theory suggests that we must cut the prism at the point $x_e = x_{max}$ to obtain the maximum coupling efficiency. However, for a more accurate determination of x_e, we should take into account the coefficient κ of energy transfer from BSW under the prism to BSW on the bare PC, which can depend on x and is defined by the overlap integral of these BSWs. For each pair of φ and d, we calculated $E(x,z)$, $\kappa(x)$ and determined maximum coupling efficiency η and corresponding $x_e - x_M$. The $\eta(\varphi, d)$ dependence shown in Figure 3b reveals a peak coupling efficiency $\eta = 77\%$ at an incidence angle $\varphi_{ex} = 46.2°$, gap thickness $d = 290$ nm, and $x_e - x_M = 5.9$ µm. Thus, the parameters found using analytical theory are very close to those obtained by numerical simulation. The 3% reduction in coupling efficiency in the simulation is caused by BSW scattering at the prism edge due to mode mismatch. A black contour in Figure 3b shows the parameter area with the coupling efficiency greater than 50%. We observe an excellent robustness of prism efficiency to fabrication errors: the gap thickness can vary
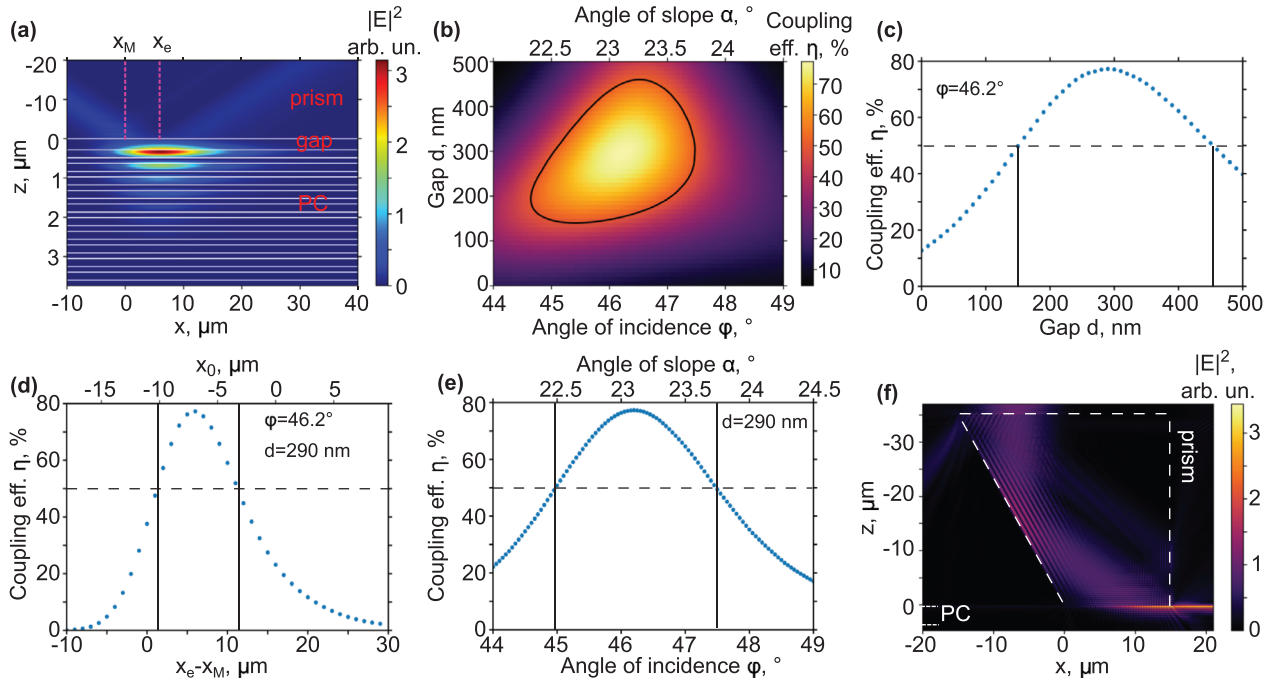
within more than 200 nm (Figure 3c), while the angle of slanted face within a degree (Figure 3e). In addition, Figure 3d shows the dependence of coupling efficiency on the beam position for the optimal case, also demonstrating the tolerance of prism couplers to beam position errors that can reach ±3 microns. Notably, the BSW excitation with $\eta > 10\%$ is possible for the case of a zero gap, when the beam hits the corner of the prism (Section S6, Supporting Information).

Finally, we verified the obtained results by performing the 2D FDTD simulation for the prism with the optimal parameters and $H = 35$ µm, $L = 16$ µm (Figure 3f). The calculated efficiency is 73%, which is 4% less than the value obtained by TMM due to the reflection of the incident beam from the upper face of the prism.

2.3. Experiment

The microprisms of various shapes with $\alpha = 23.1°$, $L = 16$ µm, $H = 28$ µm, and $d = 0 - 1$ µm were fabricated from SZ2080 photoresist on the PC surface using custom TPL setup[56] (Experimental Section and Section S7, Supporting Information). The scanning electron microscopy image of the printed prism schematized in Figure 1 is shown in **Figure 4**a. The quality of the air gap is studied using phase-sensitive optical coherence microscopy[57] (Section S8, Supporting Information). The typical profile of the base surface of the microprism with average

ADVANCED
SCIENCE NEWS

www.advancedsciencenews.com

LASER
& PHOTONICS
REVIEWS

www.lpr-journal.org

Figure 3. Verification of coupler parameters using numerical simulation. a) 2D field distribution inside the structure shown in Figure 2a with a gap $d = 290$ nm. A Gaussian beam with $\lambda_0 = 780$ nm and $w = 10$ μm is focused on the prism base at point (0, 0) and at an angle of incidence of $\varphi_{ex} = 46.2°$. Borders of photonic crystal layers and the prism base are shown with white lines. b) Dependence of coupling efficiency η on the gap thickness d and the angle of incidence $\varphi = 2\alpha$ for the optimal beam positions $x_e - x_M$. A black contour shows the parameter area in which the coupling efficiency exceeds 50%. c) Dependence of coupling efficiency η on the gap d for $\varphi = 46.2°$ at optimal beam position $x_e - x_M$ for each d. d) Dependence of coupling efficiency η on the position of the incident beam for the optimal values of $d = 290$ nm and $\varphi = 46.2°$. e) Dependence of coupling efficiency η on the angle φ for optimal $d = 290$ nm. Dashed lines in (c), (d), and (e) indicate the range of parameters for which the coupling efficiency exceeds 50%. f) Intensity distribution in the studied system calculated using FDTD for optimal parameters: $d = 290$ nm, $\varphi = 46.2°$, $\alpha = 23.1°$, and $x_e - x_M = 5.9$ μm.
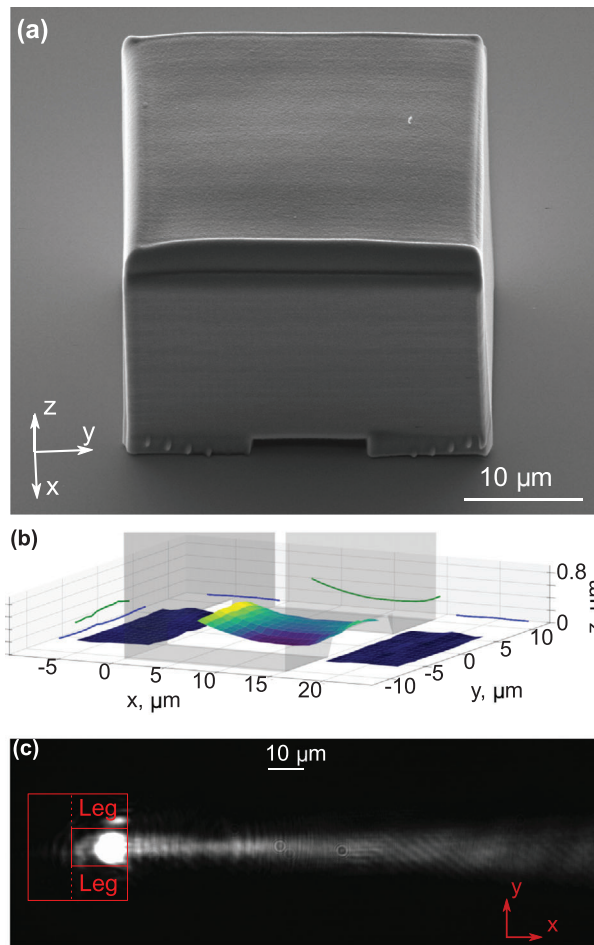
$d = 200$ nm is shown in Figure 4b. The surface is almost flat along the y-axis and is convex along the x-axis corresponding to the BSW propagation direction. The convex shape can be the result of polymer shrinkage due to a higher exposure dose in the center of the prism with respect to its edges. Nevertheless, the gap does not contain any considerable defects or roughness and can be printed up to 50 nm thick (Figure S8, Supporting Information). The observed gap nonuniformity does not significantly affect the coupling efficiency as shown in Section S9, Supporting Information.

The BSW excitation was studied using leakage radiation microscopy[10,58] (LRM) detailed in Experimental Section and Section S10, Supporting Information. By detecting radiation leaking from BSW through PC, we visualized the BSW propagation as shown in Figure 4c. We defined the BSW propagation length L_{BSW} as the distance at which the BSW intensity decreases by e times and obtained the value $L_{BSW} = 1.4 \pm 0.1$ mm. We also determined $Re(n_{eff}) = 1.097 \pm 0.010$ (Section S11, Supporting Information), which is in an excellent agreement with the theoretical value of 1.092 predicted by TMM for BSW on the bare PC.

The BSW coupling efficiency was evaluated depending on the incident beam position (x_0, y_0) by two methods. We used the prisms with two identical slanted faces ($\alpha = 23.1°$, **Figure 5**a) and measured the powers of reflected, transmitted and leaked beams depicted in Figure 5b. The first method assumes that all radiation that is not part of the transmitted or reflected radiation is coupled to BSW (Experimental Section and Section S12, Supporting In-

formation). This method provides an upper estimate for coupling efficiency giving the maximum value $\eta = 54\%$ in the experiment for the prism with $d = 300$ nm. In the second method, only the BSW leakage radiation power is measured, which is proportional to the BSW power and therefore to the coupling efficiency (Experimental Section and Section S13, Supporting Information). Due to neglect of BSW scattering, the method gives the lower estimate for η value. Figure 5c shows the $\eta(x_0, y_0)$ map obtained by the second method for the most efficient prism with $d = 300$ nm (the efficiency map obtained by the first method is shown in Figure S12, Supporting Information). The maximum efficiency of 40% is observed for $y_0 = 0$ corresponding approximately to the gap center and $x_0 = -7$ μm very close to the value predicted by the calculations (Figure 3d). The obtained efficiency is more than twice the previously reported value of 18% for the BSW platform.[51] We also observe that BSW is excited with an efficiency greater than 10% in the regions of the prism legs, as the beam reflected from the slanted face hits the corner between the leg base and the second slanted face, implementing a kind of Otto configuration with zero gap (Section S6, Supporting Information).

The upper and lower estimates of the maximum coupling efficiency obtained by scanning prisms with various gap thicknesses are shown in Figure 5d by red and blue dots, respectively. The orange curve represents the theoretical dependence of the coupling efficiency shown in Figure 3c, taking into account the reflection of the beam from the upper face of the prism. The maximum coupling efficiency in the range from 40% to 54% is observed

**ADVANCED
SCIENCE NEWS**

www.advancedsciencenews.com

LASER
& PHOTONICS
REVIEWS

www.lpr-journal.org

Figure 4. Experiment with prism couplers. a) Scanning electron microscopy image of the polymer microprism with $d = 1\,\mu m$ printed using two-photon laser lithography. b) Air gap profile with an average thickness of $d = 200$ nm measured using optical coherent microscopy. Green curves show average gap profiles along x and y axes. Blue curves show the substrate surface. The minimum gap thickness is 160 nm. c) Leakage radiation microscopy image of BSW excited by the microprism coupler with $d = 300$ nm. Laser radiation ($\lambda_0 = 780$ nm) is focused at the normal incidence on the prism into a 10 μm spot. Prism borders are shown with red lines.

at the gap thickness of 300 nm, as predicted by the theory. The lower values in the experiment are associated with light scattering by inhomogeneities on the prism surfaces, as well as with deviations in the excitation angle because of fabrication errors. We believe that the precision in microprism fabrication required to achieve the theoretical coupling efficiency is readily available for commercial TPL printers.

It is possible to focus waveguide modes simultaneously with its excitation by making the slanted face in the form of, for example, a conical mirror, as shown in **Figure 6**a. The focal length of the total reflection mirror is 40 μm and the focusing numerical aperture is 0.14. The LRM image of propagating BSW shown in Figure 6b demonstrates the BSW focusing into a diffraction limited spot $3.1 \pm 0.3\,\mu m$ in diameter (Figure 6c, Sections S7 and S11, Supporting Information). The ability to change the slanted face profile in different ways depending on the z coordinate re-

veals new interesting possibilities in beam shaping of SEWs or waveguide modes.

2.4. Discussion

To summarize, we have proposed the concept of a miniature out-of-plane prism coupler designed to couple light into waveguides on an optical chip using the Otto configuration. We have presented a method for determining the optimal parameters of the microprism with a uniform air gap for a given beam diameter and the type of photonic platform, providing the coupling efficiency up to 80%. The concept is validated on the BSW platform by coupling a 10 μm Gaussian beam to BSW using polymer microprism with a size of about 30 μm and a gap of about 300 nm, printed on the surface of a 1D photonic crystal by two-photon polymerization technique. Fabricated proof-of-concept couplers show an experimental BSW excitation efficiency of more than 40%, which exceeds significantly the previous achievement of 18% obtained using a grating for BSW excitation. Coupler performance demonstrates excellent resistance to fabrication and alignment errors as well as gap nonuniformity. In addition, we show the possibility of manipulating the waveguide mode by fabricating a coupler that focuses BSW simultaneously with its excitation.

We note some general properties of the proposed prism couplers for the case of an air gap and normal incidence. The coupler allows one to excite waveguide modes with $1 < Re(n_{eff}) < n_{pr}$ implying that the material of the prism limits the coupler applicability. In most cases this means that the prism can be made of the same material as the waveguide, since the effective refractive index of the mode with evanescent field in air is less than that of the waveguide material. In addition, subwavelength structuring allows the effective refractive index of the modes of SOI waveguides to be reduced down to 1.45,[15] making microprism couplers printed from high index ($n = 1.6^{[59]}$) photoresists potentially applicable for the SOI platform. To fulfill simultaneously the total internal reflection conditions on the slanted face and on the prism base, the slope angle α must fall within the range $\pi/2 - \arcsin(1/n_{pr}) > \alpha > \arcsin(1/n_{pr})/2$. Hence the coupler starts functioning at , and the excitation of waveguide modes in the entire possible range of effective refractive indexes becomes available at , as the maximum slope angle reaches 45°. Both conditions are easily met in the visible and IR ranges for almost any transparent material, making the choice of prism material dependent only on the maximum $Re(n_{eff})$ of the waveguide mode to be excited.

Microprism couplers possess several advantages over diffraction gratings. First, directionality of gratings is considerably less than 100%, that is, part of the waveguide mode energy is always directed by the grating into the substrate,[16] which is not the case for prism couplers. To increase the grating directionality, special techniques such as backreflectors should be applied,[16] which makes grating fabrication more complex. Second, state-of-the-art coupling efficiency is demonstrated for an incidence angle of about 10°,[24,28] while perfectly vertical grating couplers are significantly less efficient.[60] Contrary, by varying the angle of the slanted face, the microprism can be flexibly adjusted for any angle of incidence, including the normal one, without affecting the coupling efficiency. Third, all high-performance gratings
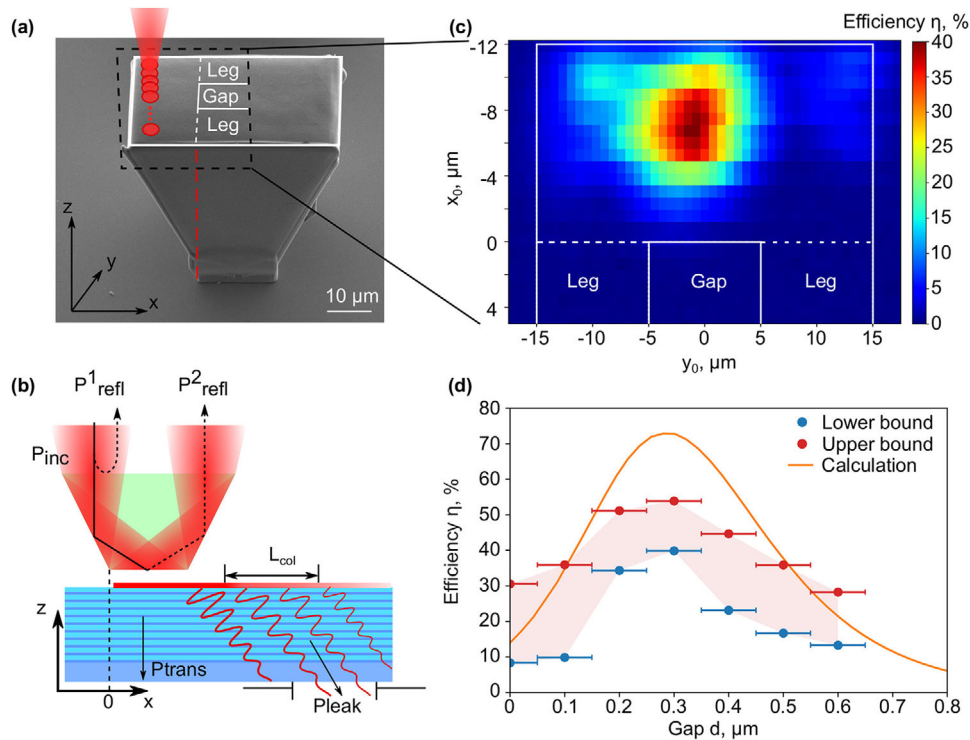
Figure 5. Coupling efficiency measurements. a) Scanning electron microscopy image of the polymer microprism with two identical slanted faces ($\alpha = 23.1°$). The prism is scanned by the incident beam in the area indicated by black dashed lines. b) Schematic of the experiment for determining the coupling efficiency. The powers of incident (P_{inc}), reflected (P^1_{refl}, P^2_{refl}), transmitted (P_{trans}), and leaked (P_{leak}) beams are measured for each position (x_0, y_0) of the incident beam. c) The coupling efficiency $\eta(x_0, y_0)$ obtained by measuring the BSW leakage radiation power $P_{leak}(x_0, y_0)$, which is proportional to η. Prism borders are shown with white lines. d) Coupling efficiency measured versus gap thickness d. Red and blue dots show the upper and lower estimates of the coupling efficiency. An orange curve is the calculated dependence shown in the Figure 3c, taking into account the losses due to reflection of the incident beam from the upper face of the prism.
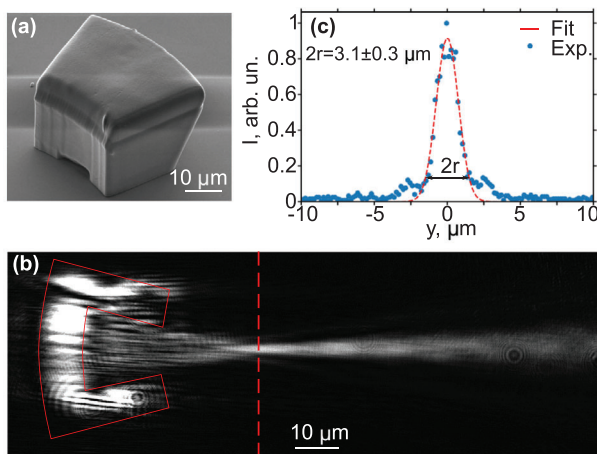
Figure 6. Demonstration of the focusing coupler. a) Scanning electron microscopy image of the microprism with the slanted face in the form of a conical mirror with a focus length of 40 μm. b) LRM image of the BSW propagation. Prism borders are shown with red lines. c) BSW intensity distribution in the focal plane shown by the red dashed line in panel (b). Experimental data are shown with blue dots. Red dashed curve is the result of approximation with Gaussian function.

have been demonstrated for the SOI platform. They operate in the telecommunication range, possess high optical contrast and a minimum element size of down to 100 nm.[25,28] As a result, the scaling of the grating technique into the visible or near-IR ranges faces great technological challenges, if at all possible. Microprisms can be easily fabricated to operate in the visible range, since even then they require a gap of several hundred nanometers thick. In addition, the coupling efficiency of the prisms is not limited to optical contrast, meaning that they are perfectly suited for low index platforms such as BSW and SPP platforms. The footprint of the prism is determined by the lateral dimensions of the gap, which, as in the case of gratings, is equal to the size of the incident beam, taking into account, however, that the length of the gap is increased by a factor of $1/\cos(\varphi_{ex})$. Together with the legs and the inclined face, a typical microprism coupler will be two to three times larger than the grating. Additive technologies provide many additional advantages. For example, microprisms can be fabricated simultaneously with fiber holders,[61] providing micron control of the beam position x_0 on the prism and a robust optical connection. Also, the prism can be created initially on the end of the fiber[62] and attached to the photonic platform in arbitrary places, realizing a kind of probe for diagnosing photonic circuits. To inject light into a photonic circuit, the microprism coupler can be fabricated over a wide waveguide, which is further tapered to the size of a single-mode waveguide. The ability

**ADVANCED
SCIENCE NEWS**

www.advancedsciencenews.com

LASER
& PHOTONICS
REVIEWS

www.lpr-journal.org

to focus light with the prism provides additional flexibility in photonic chip design.

The main idea of the Otto configuration, which makes its use in integrated photonics extremely attractive, is the controlled broadening of the waveguide mode angular resonance to the divergence of the focused incident beam, thus coupling all spatial components of the beam to the mode. This approach is particularly relevant for the excitation of high-Q waveguide modes whose resonances are much narrower than the divergence of radiation emerging, for example, from conventional single-mode fiber. The angular resonance width is adjusted by varying the gap thickness, which in the case of TPL printing is controlled with nanometer precision by a conventional piezo stage without resorting to complex techniques such as focused electron beams. The application of the prism microcouplers is not limited to the integrated photonics. Conventional Otto configuration is successfully applied for sensing,[63,64] and the proposed microprisms can be used as integrated microsensors operating at normal angle of incidence. Another potential application is surface wave resonance microscopy,[42] where a set of microprisms can be used to illuminate the area of interest from all directions.

Finally, the limitations in maximum coupling efficiency indicated for the uniform gap can be overcome, bringing the efficiency close to 100% without affecting the microprism size. The easiest way is to implement a wedge gap, the thickness of which increases in the direction of waveguide mode propagation.[53] An increase in thickness leads to a decrease in the decoupling process and adiabatically brings the parameters of the mode under the prism to the parameters of the mode outside the prism, avoiding the mode mismatch scattering by analogy with adiabatic tapers.[65] With proper optimization of the TPL process, creating a wedge-gap prism should not be very complex.

3. Experimental Section

BSW Platform and Prism Printing: PC was designed to sustain TE-polarized BSW at 780 nm and composed of ten bilayers sputtered on top of a glass substrate (170 µm thickness, $n_{glass} = 1.52$). Each bilayer consisted of a 204 nm thick SiO_2 layer ($n_{SiO_2} = 1.45$ at $\lambda = 780$ nm) and 142 nm thick Ta_2O_5 layer ($n_{Ta_2O_5} = 2.07$ at $\lambda = 780$ nm). The terminating layer is SiO_2, which enabled BSW excitation on a bare PC.

Microprisms were printed on top of the PC using custom two-photon laser lithography setup[56] based on Ti:Sapphire laser (Coherent Chameleon, $\lambda = 780$ nm, 150 fs pulse duration, 80 MHz repetition rate). A droplet of SZ2080 photoresist was placed on the PC surface and baked for 45 min at 95 °C to evaporate the solvent. Using an oil-immersion objective lens (NA = 1.3, 100×, Olympus), the laser beam was focused into the photoresist through the PC (Figure S6a, Supporting Information) that is transparent to the wavelength of the exposure radiation. The beam waist was moved in the sample (*xy*) plane using a fast steering mirror (Newport FSM300) and in the vertical (*z*) direction using a piezo stage (Newport NPO250SG), providing layer-by-layer printing of a prism from bottom to top in about 9 min. The computer models of all prisms had a gap of 5 µm (Figure S6b–d, Supporting Information). The gap between the prism base and PC surface was adjusted by shifting the lower point of the model into PC by value z_{shift}. Before printing each prism, the dependence of two-photon luminescence signal of the photoresist was automatically measured on the *z*-position of the beam waist during its movement across the PC surface. The waist position corresponding to the maximum of the derivative of the obtained dependence was taken as the reference,[66] from which the model was shifted by z_{shift}. The set of prisms with various gaps

was printed on a common PC in a single exposure procedure when the z_{shift} value was changed by 100 nm from prism to prism. The printed structures were developed in methyl isobutyl ketone during 12–14 h using an orbital shaker and then rinsed with isopropyl alcohol.

Transfer Matrix Method with Plane Wave Expansion: Using general method, the optimal parameters of the prism coupler for the case $w \gg \lambda_0$ can be quite accurately determined, where λ_0 is the wavelength of light incident on the prism. However, 2D calculations are required to refine the optimal coupling parameters in cases of tight focusing, as well as to determine the coupling efficiency and the effect of fabrication and beam positioning errors on it. Here, TMM was complemented with a plane wave expansion approach for performing 2D calculations in layered structures with parallel boundaries that are typical of most waveguide platforms. The method works for nonparallel (i.e., focused or divergent) beams and is more accurate and much faster than Lumerical FDTD in the case of a large number of interfaces (Section S5, Supporting information).

In its own coordinate system (x', z'), the incident Gaussian beam field was represented through the Fourier transform as a set of plane waves

$$E(x', z') = \int S(k_{x'})e^{ik_{x'}x' + ik_{z'}z'}\,dk_{x'} \tag{4}$$

with amplitudes corresponding to the angular spectrum of the beam

$$S(k_{x'}) = \frac{\sqrt{w}}{2\sqrt{\pi}}e^{-\left(\frac{wk_{x'}}{2}\right)^2} \tag{5}$$

where $k_{z'} = \sqrt{k^2 - k_{x'}^2}$, $k = 2\pi n_{pr}/\lambda_0$ is the wavevector in the prism. The coefficient $\sqrt{w}/2\sqrt{\pi}$ ensured that the same beam power $P_{inc} \approx \int |E(x')|^2 dx'$ was maintained for different beam widths w. For calculations, the parameters k_x and $S(k_x)$ of the incident beam were taken in the sample coordinate system (x, z) that is rotated by the angle of incidence φ relative to the beam coordinate system (x', z'). TMM was used to obtain the electric field distribution $E(z)$ for each k_x, that is, to find $E(k_x, z)$. Next, the 2D field distribution was calculated

$$E(x, z) = \int E(k_x, z)S(k_x)e^{ik_x x + i\sqrt{k^2 - k_x^2}z}\,dk_x \tag{6}$$

an example of which is shown in Figure 3a. Now, for each position x_e of the prism edge, the coupling efficiency can be found as

$$\eta(x_e) = \kappa(x_e)P(x_e)/P_{inc} \tag{7}$$

where $P(x_e)$ is the total power of the surface wave at the prism edge, and $\kappa(x_e)$ is a coefficient indicating what part of the energy of BSW under the prism is transferred to BSW on the bare PC. The BSW power was calculated as the flux of the Poynting vector through the cross section of PC

$$P(x) = \int \frac{c}{4\pi}[\vec{E} \times \vec{H}]_x\,dz \tag{8}$$

$\vec{H}(x, z)$ can be obtained through the Fourier transform using amplitudes $\vec{H}(k_x, z) = n(z)\,S(k_x)\,[\vec{E}(k_x, z) \times \vec{k}(k_x, z)]\frac{1}{|\vec{k}(k_x, z)|}$, where $n(z)$ is the refractive index of the layer with coordinate z. $\kappa(x)$ was found by calculating the overlap integral of the BSW field distribution under the prism and the field distribution E_{BSW} of BSW on the bare PC surface

$$\kappa(x) = \frac{|\int E^*(x, z)E_{BSW}\,dz|^2}{\int |E(x, z)|^2 dz \int |E_{BSW}|^2 dz} \tag{9}$$

From the dependence $\eta(x_e)$, an example of which is shown in Figure 3d, the maximum coupling efficiency and the corresponding value of $x_e - x_M$ were found. Repeating the calculation procedure for each φ and d, the dependence of maximum efficiency $\eta(\varphi, d)$ shown in Figure 3b was found.

**ADVANCED
SCIENCE NEWS**

www.advancedsciencenews.com

LASER
& PHOTONICS
REVIEWS

www.lpr-journal.org

Leakage Radiation Microscopy: During the BSW propagation along the PC surface, part of its energy is lost in the form of radiation leaking through PC into the substrate at an angle θ corresponding to the phase-matching condition $n_{sb} \sin \theta = Re(n_{eff})$, where n_{sb} is the substrate refractive index. This leakage radiation can be collected using an objective lens with NA > $Re(n_{eff})$. Leakage radiation intensity is proportional to the BSW intensity. As a result, BSW can be visualized and its parameters can be measured by filtering the radiation in the k-space and directing only the BSW leakage radiation to the detector.

The scheme and details of the LRM setup are described in Section S10, Supporting Information. Radiation from a 780 nm laser diode was focused in the back focal plane of an air objective lens (NA = 0.95, 100×), which then focused the beam on the prism base into a 10 μm spot. Polarization of incoming light was set perpendicular to the long side of the gap. The transmitted and BSW leakage radiation was collected by an oil-immersion objective lens (NA = 1.3, 100×, Olympus), while the reflected and backscattered radiation was collected by the focusing air objective lens. Thus, all radiation was collected except for the beams scattered at angles of 0–20° to the PC surface. The transmitted radiation was filtered using an aperture and a slit set in the intermediate images of front and back focal plane of the oil-immersion objective lens, respectively. After filtering, the front and back focal plane images were simultaneously rebuilt on two CMOS cameras. The image of the PC surface obtained by the focusing air objective lens was detected by the third CMOS camera, allowing to observe the reflected beams. The powers of the transmitted and reflected beams were measured simultaneously using two identical Si photodiodes.

Coupling Efficiency Measurements: The prisms with two identical slanted faces were used. In this case, the total radiation reflected from the prism (P_{refl}) is the sum of two reflected beams with powers P_{refl}^1 and P_{refl}^2 (Figure 5b). P_{refl}^1 corresponds to the radiation directly reflected from the upper prism face. P_{refl}^2 is a part of the incident radiation that did not transfer into BSW, undergoing one additional total internal reflection on the second slanted face and leaving the prism in a direction parallel to the incident beam. The use of spatial filtering made it possible to independently measure the power of transmitted radiation (P_{trans}) and BSW leakage radiation (P_{leak}).

To determine the efficiency by the first method, the dependences of reflection coefficient $R = P_{refl}/P_{inc}$ and transmission coefficient $T = P_{trans}/P_{inc}$ were measured on the position (x_0, y_0) of the beam when it was scanning the prism and a part of the bare PC around the prism. First, using a bare cover glass as a reference sample with known reflectance and transmittance, the transmission and reflection coefficients t and r of all optical elements of the setup in the transmission and reflection channels, correspondingly, were found. Then the power of the radiation transmitted through (P_{trans}^{PC}) and reflected from (P_{refl}^{PC}) the bare PC was measured to determine the PC transmittance $T^{PC} = P_{trans}^{PC}/(P_{inc}t)$ and reflectance $R^{PC} = P_{refl}^{PC}/(P_{inc}r)$, where P_{inc} is the power of the beam incident on the prism. With a known PC reflection and transmission coefficients, power of the incident beam can be determined by measuring P_{trans}^{PC} and P_{refl}^{PC} during the scanning of prisms using the signal from the areas of the bare PC. For example, in the case of reflection, $P_{inc} = P_{refl}^{PC}/(R^{PC}r)$. The measured power of the radiation reflected from the prism is $P_{refl}(x_0, y_0) = P_{inc}rR(x_0, y_0) = P_{refl}^{PC}R(x_0, y_0)/R^{PC}$, where $R(x_0, y_0)$ is reflectance of the prism at the measurement point (x_0, y_0). From this, $R(x_0, y_0) = R^{PC}P_{refl}(x_0, y_0)/P_{refl}^{PC}$ and, by analogy, $T(x_0, y_0) = T^{PC}P_{trans}(x_0, y_0)/P_{trans}^{PC}$, where $P_{trans}(x_0, y_0)$ is the measured power of the radiation transmitted through the prism (leakage radiation is blocked and not measured). Finally, the coupling efficiency was determined as $\eta(x_0, y_0) = 1 - R(x_0, y_0) - T(x_0, y_0)$, which means that all radiation that is not part of the transmitted or reflected radiation is considered to be coupled to BSW. This method gave an upper estimate of the coupling efficiency because it does not account for scattering light propagating along the PC surface and not being collected by the focusing objective lens. Additional information is provided in Section S12, Supporting Information.

In the second method, only the power P_{leak} of the BSW leakage radiation was measured when scanning the prism with the incident beam and the

BSW leakage transmission coefficient $T_{leak} = P_{leak}/P_{inc}$ was determined. In all the experiments, the BSW leakage radiation was collected from a circular region of the bare PC with a radius of 50 μm, centered in the direction of BSW propagation at a distance of 70 μm from the gap edge (Figure S10, Supporting Information). The leakage radiation energy is proportional to the light energy in BSW and depends only on the structure of PC, mainly on the number of PC layers.[67] Therefore, at a constant power of the incident beam, the power of the BSW leakage radiation depends only on the prism coupling efficiency. Assuming that the BSW attenuation is caused by two processes—leakage and absorption,—the leakage transmission coefficient is $T_{leak} = \eta L_{col}(1/L_{BSW} - 1/L_{abs})$, where L_{col} is the length of the collection area, L_{BSW}—BSW propagation length, and $L_{abs} = 1/(k_0 n'')$—absorption length in PC materials with an imaginary part of the refractive index of n'' (derivation of this equation is given in Section S13, Supporting Information). In this case, $L_{col} = 100$ μm, $L_{BSW} = 1.4 \pm 0.1$ mm, and $n'' \approx 10^{-5}$ resulting in $L_{abs} \approx 12$ mm. Thus, coupling efficiency η can be estimated by the value of T_{leak}

$$\eta = T_{leak} \frac{L_{BSW}}{L_{col}} \frac{1}{1 - L_{BSW}/L_{abs}} \qquad (10)$$

This type of estimation gave a lower bound of efficiency, since the BSW attenuation related to scattering was not taken into account. Accounting for the contribution of scattering will increase the last multiplier in the formula.

Supporting Information

Supporting Information is available from the Wiley Online Library or from the author.

Acknowledgements

Conflict of Interest

The authors declare no conflict of interest.

Data Availability Statement

The data that support the findings of this study are available from the corresponding author upon reasonable request.

Keywords

ADVANCED SCIENCE NEWS

www.advancedsciencenews.com

LASER & PHOTONICS REVIEWS

www.lpr-journal.org

[1] M. C. Estevez, M. Alvarez, L. M. Lechuga, *Laser Photonics Rev.* **2012**, 6, 463.

[2] J. Wang, S. Paesani, Y. Ding, R. Santagati, P. Skrzypczyk, A. Salavrakos, J. Tura, R. Augusiak, L. Mančinska, D. Bacco, D. Bonneau, J. W. Silverstone, Q. Gong, A. Acín, K. Rottwitt, J. L. Oxenløwe, Leif K.and O'Brien, A. Laing, M. G. Thompson, *Science* **2018**, 360, 285.

[3] Y. Shen, N. C. Harris, S. Skirlo, M. Prabhu, T. Baehr-Jones, M. Hochberg, X. Sun, S. Zhao, H. Larochelle, D. Englund, M. Soljačić, *Nat. Photonics* **2017**, 11, 441.

[4] W. Bogaerts, R. Baets, P. Dumon, V. Wiaux, S. Beckx, D. Taillaert, B. Luyssaert, J. Van Campenhout, P. Bienstman, D. Van Thourhout, *J. Light. Technol.* **2005**, 23, 401.

[5] A. Politi, M. J. Cryan, J. G. Rarity, S. Yu, J. L. O'brien, *Science* **2008**, 320, 646.

[6] A. Rahim, E. Ryckeboer, A. Z. Subramanian, S. Clemmen, B. Kuyken, A. Dhakal, A. Raza, A. Hermans, M. Muneeb, S. Dhoore, Y. Li, U. Dave, P. Bienstman, N. L. Thomas, G. Roelkens, D. Van Thourhout, P. Helin, S. Severi, X. Rottenberg, R. Baets, *J. Light. Technol.* **2017**, 35, 639.

[7] H. Raether, in *Surface Plasmons on Smooth and Rough Surfaces and on Gratings*, Springer, Berlin, Heidelberg **1988**, pp. 4–39.

[8] P. Yeh, A. Yariv, A. Cho, *Appl. Phys. Lett.* **1978**, 32, 104.

[9] R. F. Oulton, V. J. Sorger, D. Genov, D. Pile, X. Zhang, *Nat. Photonics* **2008**, 2, 496.

[10] K. R. Safronov, D. N. Gulkin, I. M. Antropov, K. A. Abrashitova, V. O. Bessonov, A. A. Fedyanin, *ACS Nano* **2020**, 14, 10428.

[11] L. Liu, Z. Han, S. He, *Opt. Express* **2005**, 13, 6645.

[12] P. Berini, R. Charbonneau, N. Lahoud, G. Mattiussi, *J. Appl. Phys.* **2005**, 98, 043109.

[13] B. B. Bakir, A. V. De Gyves, R. Orobtchouk, P. Lyan, C. Porzier, A. Roman, J.-M. Fedeli, *IEEE Photonics Technol. Lett.* **2010**, 22, 739.

[14] T. Barwicz, B. Peng, R. Leidy, A. Janta-Polczynski, T. Houghton, M. Khater, S. Kamlapurkar, S. Engelmann, P. Fortier, N. Boyer, W. M. J. Green, *IEEE J. Sel. Top. Quantum Electron.* **2018**, 25, 4700313.

[15] P. Cheben, J. H. Schmid, S. Wang, D.-X. Xu, M. Vachon, S. Janz, J. Lapointe, Y. Painchaud, M.-J. Picard, *Opt. Express* **2015**, 23, 22553.

[16] R. Marchetti, C. Lacava, L. Carroll, K. Gradkowski, P. Minzioni, *Photonics Res.* **2019**, 7, 201.

[17] P.-I. Dietrich, M. Blaicher, I. Reuter, M. Billah, T. Hoose, A. Hofmann, C. Caer, R. Dangel, B. Offrein, U. Troppenz, *Nat. Photonics* **2018**, 12, 241.

[18] T. Yoshida, E. Omoda, Y. Atsumi, T. Nishi, S. Tajima, R. Takei, N. Miura, M. Mori, Y. Sakakibara, in *Integrated Photonics Research, Silicon and Nanophotonics*, Optical Society of America, Washington, DC **2016**, p. ITu2B–1.

[19] H. Gehring, M. Blaicher, W. Hartmann, P. Varytis, K. Busch, M. Wegener, W. Pernice, *APL Photonics* **2019**, 4, 010801.

[20] H. Luo, F. Xie, Y. Cao, S. Yu, L. Chen, X. Cai, *Opt. Lett.* **2020**, 45, 1236.

[21] H. Gehring, A. Eich, C. Schuck, W. H. Pernice, *Opt. Lett.* **2019**, 44, 5089.

[22] R. Marchetti, C. Lacava, A. Khokhar, X. Chen, I. Cristiani, D. J. Richardson, G. T. Reed, P. Petropoulos, P. Minzioni, *Sci. Rep.* **2017**, 7, 16670.

[23] X. Chen, C. Li, C. K. Fung, S. M. Lo, H. K. Tsang, *IEEE Photonics Technol. Lett.* **2010**, 22, 1156.

[24] Y. Ding, C. Peucheret, H. Ou, K. Yvind, *Opt. Lett.* **2014**, 39, 5348.

[25] D. Benedikovic, P. Cheben, J. H. Schmid, D.-X. Xu, J. Lapointe, S. Wang, R. Halir, A. Ortega-Moñux, S. Janz, M. Dado, *Laser Photonics Rev.* **2014**, 8, L93.

[26] D. Benedikovic, C. Alonso-Ramos, S. Guerber, X. Le Roux, P. Cheben, C. Dupre, B. Szelag, D. Fowler, E. Cassan, D. Marris-Morini, C. Baudot, F. Boeuf, L. Vivien, *Opt. Express* **2019**, 27, 26239.

[27] X. Wen, K. Xu, Q. Song, *Photonics Res.* **2016**, 4, 209.

[28] W. S. Zaoui, A. Kunze, W. Vogel, M. Berroth, J. Butschke, F. Letzkus, J. Burghartz, *Opt. Express* **2014**, 22, 1277.

[29] D. Sarid, P. J. Cressman, R. L. Holman, *Appl. Phys. Lett.* **1978**, 33, 514.

[30] Z. Lu, D. W. Prather, *Opt. Lett.* **2004**, 29, 1748.

[31] A. Sánchez-Postigo, R. Halir, J. G. Wangüemert-Pérez, A. Ortega-Moñux, S. Wang, M. Vachon, J. H. Schmid, D.-X. Xu, P. Cheben, Í. Molina-Fernández, *Laser Photonics Rev.* **2021**, 15, 2000542.

[32] E. Kretschmann, H. Raether, *Z. Naturforsch. A* **1968**, 23, 2135.

[33] A. Otto, *Z. Phys. A Hadrons Nucl.* **1968**, 216, 398.

[34] R. Dubey, E. Barakat, M. Häyrinen, M. Roussey, S. Honkanen, M. Kuittinen, H. P. Herzig, *J. Eur. Opt. Soc.-Rapid* **2017**, 13, 5.

[35] R. Badugu, J. Mao, S. Blair, D. Zhang, E. Descrovi, A. Angelini, Y. Huo, J. R. Lakowicz, *J. Phys. Chem. C* **2016**, 120, 28727.

[36] G. M. Smolik, N. Descharmes, H. P. Herzig, *ACS Photonics* **2018**, 5, 1164.

[37] R. Dubey, B. V. Lahijani, E. Barakat, M. Häyrinen, M. Roussey, M. Kuittinen, H. P. Herzig, *Opt. Lett.* **2016**, 41, 4867.

[38] L. Yu, E. Barakat, T. Sfez, L. Hvozdara, J. Di Francesco, H. P. Herzig, *Light Sci. Appl.* **2014**, 3, e124.

[39] D. N. Gulkin, A. A. Popkova, B. I. Afinogenov, D. A. Shilkin, K. Kuršelis, B. N. Chichkov, V. O. Bessonov, A. A. Fedyanin, *Nanophotonics* **2021**, 10, 2939.

[40] A. Sinibaldi, A. Fieramosca, R. Rizzo, A. Anopchenko, N. Danz, P. Munzert, C. Magistris, C. Barolo, F. Michelotti, *Opt. Lett.* **2014**, 39, 2947.

[41] A. L. Lereu, M. Zerrad, A. Passian, C. Amra, *Appl. Phys. Lett.* **2017**, 111, 011107.

[42] Y. Kuai, J. Chen, X. Tang, Y. Xiang, F. Lu, C. Kuang, L. Xu, W. Shen, J. Cheng, H. Gui, G. Zou, P. Wang, H. Ming, J. Liu, X. Liu, J. R. Lakowicz, D. Zhang, *Sci. Adv.* **2019**, 5, eaav5335.

[43] D. A. Shilkin, E. V. Lyubin, I. V. Soboleva, A. A. Fedyanin, *Opt. Lett.* **2015**, 40, 4883.

[44] M. N. Romodina, I. V. Soboleva, A. I. Musorin, Y. Nakamura, M. Inoue, A. A. Fedyanin, *Phys. Rev. B* **2017**, 96, 081401.

[45] V. N. Konopsky, E. V. Alieva, S. Y. Alyatkin, A. A. Melnikov, S. V. Chekalin, V. M. Agranovich, *Light Sci. Appl.* **2016**, 5, e16168.

[46] I. V. Soboleva, E. Descrovi, C. Summonte, A. A. Fedyanin, F. Giorgis, *Appl. Phys. Lett.* **2009**, 94, 231122.

[47] F. Barachati, A. Fieramosca, S. Hafezian, J. Gu, B. Chakraborty, D. Ballarini, L. Martinu, V. Menon, D. Sanvitto, S. Kéna-Cohen, *Nat. Nanotechnol.* **2018**, 13, 906.

[48] G. Lerario, D. Ballarini, A. Fieramosca, A. Cannavale, A. Genco, F. Mangione, S. Gambino, L. Dominici, M. De Giorgi, G. Gigli, D. Sanvitto, *Light Sci. Appl.* **2017**, 6, e16212.

[49] I. V. Soboleva, V. V. Moskalenko, A. A. Fedyanin, *Phys. Rev. Lett.* **2012**, 108, 123901.

[50] M. Malinauskas, M. Farsari, A. Piskarskas, S. Juodkazis, *Phys. Rep.* **2013**, 533, 1.

[51] T. Kovalevich, P. Boyer, M. Suarez, R. Salut, M. Kim, H. P. Herzig, M. Bernal, T. Grosjean, *Opt. Express* **2017**, 25, 5710.

[52] R. Ulrich, *J. Opt. Soc. Am.* **1970**, 60, 1337.

[53] R. Ulrich, *J. Opt. Soc. Am.* **1971**, 61, 1467.

[54] D. Bethune, *JJ. Opt. Soc. Am. B* **1989**, 6, 910.

[55] A. Ovsianikov, J. Viertl, B. Chichkov, M. Oubaha, B. MacCraith, I. Sakellari, A. Giakoumaki, D. Gray, M. Vamvakaki, M. Farsari, C. Fotakis, *ACS Nano* **2008**, 2, 2257.

[56] K. A. Abrashitova, D. N. Gulkin, K. R. Safronov, N. G. Kokareva, I. M. Antropov, V. O. Bessonov, A. A. Fedyanin, *Appl. Sci.* **2018**, 8, 63.

[57] C. Joo, T. Akkin, B. Cense, B. H. Park, J. F. De Boer, *Opt. Lett.* **2005**, 30, 2131.

[58] A. Hohenau, J. Krenn, A. Drezet, O. Mollet, S. Huant, C. Genet, B. Stein, T. Ebbesen, *Opt. Express* **2011**, 19, 25749.

[59] M. Schmid, D. Ludescher, H. Giessen, *Opt. Mater. Express* **2019**, 9, 4564.

[60] T. Watanabe, M. Ayata, U. Koch, Y. Fedoryshyn, J. Leuthold, *J. Light. Technol.* **2017**, 35, 4663.

Laser Photonics Rev. **2022**, 16, 2100542

2100542 (10 of 11)

© 2022 Wiley-VCH GmbH

[61] O. A. J. Gordillo, S. Chaitanya, Y.-C. Chang, U. D. Dave, A. Mohanty, M. Lipson, *Opt. Express* **2019**, *27*, 20305.

[62] T. Gissibl, S. Thiele, A. Herkommer, H. Giessen, *Nat. Commun.* **2016**, *7*, 11763.

[63] E. Descrovi, F. Frascella, B. Sciacca, F. Geobaldo, L. Dominici, F. Michelotti, *Appl. Phys. Lett.* **2007**, *91*, 241109.

[64] F. Michelotti, B. Sciacca, L. Dominici, M. Quaglio, E. Descrovi, F. Giorgis, F. Geobaldo, *Phys. Chem. Chem. Phys.* **2010**, *12*, 502.

[65] Y. Fu, T. Ye, W. Tang, T. Chu, *Photonics Res.* **2014**, *2*, A41.

[66] B. J. Jung, H. J. Kong, B. G. Jeon, D.-Y. Yang, Y. Son, K.-S. Lee, *Opt. Express* **2011**, *19*, 22659.

[67] F. I. Baida, M.-P. Bernal, *Commun. Phys.* **2020**, *3*, 86.